

# CFHTLS weak-lensing constraints on the neutrino masses<sup>★</sup>

I. Tereno<sup>1,2</sup>, C. Schimd<sup>3,4</sup>, J.-P. Uzan<sup>2</sup>, M. Kilbinger<sup>2</sup>, F. H. Vincent<sup>2</sup>, and L. Fu<sup>5,6</sup>

<sup>1</sup> Argelander-Institut für Astronomie, Auf dem Hügel 71, 53121 Bonn, Germany  
e-mail: tereno@astro.uni-bonn.de

<sup>2</sup> Institut d’Astrophysique de Paris, CNRS UMR 7095 & UPMC, 98 bis bd Arago, 75014 Paris, France

<sup>3</sup> Laboratoire d’Astrophysique de Marseille, 38 rue Joliot-Curie, 13388 Marseille, France

<sup>4</sup> Université de Provence – Aix - Marseille I, Marseille, France

<sup>5</sup> INAF – Osservatorio Astronomico di Capodimonte, via Moiariello 16, 80131 Napoli, Italy

<sup>6</sup> Shanghai Key Lab for Astrophysics, Shanghai Normal University, 200234 Shanghai, PR China

Received 3 October 2008 / Accepted 7 February 2009

## ABSTRACT

**Context.** Oscillation experiments yield strong evidence that at least some neutrinos are massive. As a hot dark-matter component, massive neutrinos should modify the expansion history of the Universe as well as the evolution of cosmological perturbations, in a different way from cold dark matter or dark energy.

**Aims.** We use the latest release of CFHTLS cosmic-shear data to constrain the sum of the masses  $\sum m_\nu$  of neutrinos, assuming three degenerate mass states. We also consider a joint analysis including other cosmological observables, notably CMB anisotropies, baryonic acoustic oscillations, and distance modulus from type Ia supernovae.

**Methods.** Combining CAMB with a lensing code, we compute the aperture mass variance using a suitable recipe to deal with matter perturbations in the non-linear regime. The statistical analysis is performed by sampling an 8-dimensional likelihood on a regular grid as well as using the importance sampling technique.

**Results.** We obtain the first constraint on neutrino masses based on cosmic-shear data, and combine CFHTLS with WMAP, SDSS, 2dFGRS, Gold-set, and SNLS data. The joint analysis yields  $0.03 \text{ eV} < \sum m_\nu < 0.54 \text{ eV}$  at the 95% confidence level. The preference for massive neutrinos vanishes when systematics are included.

**Key words.** cosmology: cosmological parameters – neutrinos – cosmology: large-scale structure of Universe – gravitational lensing

## 1. Introduction

The construction of a cosmological model (Bondi 1960; Ellis 1971), must take into account any progress in the understanding of the laws of physics. To date, the reference model  $\Lambda$ CDM is based on the standard model of particle physics, general relativity, and some additional hypothesis about the symmetries of the background spacetime (the Copernican principle) to which it is mandatory to add the two still unknown components of cold dark matter (CDM) and cosmological constant ( $\Lambda$ ).

We know now that it is imperative to include the effects of massive neutrinos, which behave as a warm or hot dark matter component depending on their mass. Strong evidence of such particles, which have not yet been included in the standard model of particle physics but whose existence is supported by e.g. grand-unified theories (Calibbi et al. 2006), emerges from experimental results on oscillations of atmospheric, solar, and accelerator- or reactor-produced neutrinos, such as Super-Kamiokande, K2K, MINOS, KamLAND (see Gonzalez-Garcia & Maltoni 2008, for a review). These

results indicate a mixing of the three known neutrinos species by non-vanishing squared mass differences between the mass eigenstates and the non-vanishing corresponding mixing angles. The most recent results are  $\Delta m_{12}^2 \sim 8 \times 10^{-5} \text{ eV}^2$ ,  $\Delta m_{23}^2 \sim 2 \times 10^{-3} \text{ eV}^2$ , and mixing angles of  $\theta_{12} \sim 30^\circ$ ,  $\theta_{23} \sim 45^\circ$ , and  $\theta_{13} \lesssim 11^\circ$ . These values yield a lower bound on the heavier mass of order 0.06 (0.1) eV for normal (inverted) hierarchy, but cannot give the absolute mass scale. Forthcoming experiments based on other mechanisms, such as SuperNEMO (conceived to detect the neutrinoless double  $\beta$  decay) and KATRIN (designed to probe the tritium  $\beta$  decay) are designed to measure directly the absolute mass of the electron neutrino with a sensitivity of 0.05 and 0.2 eV, respectively.

Cosmological observations are compelling in providing an independent way to probe the absolute neutrino mass. The effect of light massive fermions in cosmology is well understood (see Lesgourgues & Pastor 2006, for a review). The standard cosmological model predicts the existence of relic neutrinos that decouple from the primeval plasma while ultra-relativistic and produce a cosmic neutrino background, which cannot yet be detected directly. Their contribution to the total radiation energy density is a fraction  $7/8(T_\nu/T_\gamma)^4 N_{\text{eff}}$  of the contribution of photons,  $T_\nu$  and  $T_\gamma$  being the temperatures of the neutrino and the photon backgrounds, respectively. The effective number of neutrinos is constrained to be  $N_{\text{eff}} = 3.04$ , if there are no extra relativistic degrees of freedom besides three active neutrinos (Mangano et al. 2002), and has an impact mainly on the primordial nucleosynthesis and the time of matter-radiation equality.

<sup>★</sup> Based on observations obtained with MegaPrime/MegaCam, a joint project of CFHT and CEA/DAPNIA, at the Canada-France-Hawaii Telescope (CFHT) which is operated by the National Research Council (NRC) of Canada, the Institut National des Sciences de l’Univers of the Centre National de la Recherche Scientifique (CNRS) of France, and the University of Hawaii. This work is based in part on data products produced at TERAPIX and the Canadian Astronomy Data Centre as part of the Canada-France-Hawaii Telescope Legacy Survey, a collaborative project of NRC and CNRS.

Analyses of light element abundances (Cuoco et al. 2004) and of the time of equality (Komatsu et al. 2009) produce results that agree with this value.

When neutrinos become non-relativistic, their velocities begin to decrease from  $c$  as  $T_\nu(t)$ , due to momentum conservation. Assuming that the mass states are degenerate ( $m_1 = m_2 = m_3 \equiv m_\nu$ ), the velocity is given by  $v_{\text{th}} = 3k_B T_\nu(t)/m_\nu c$  or, since  $T_\nu(z) \approx 1.9(1+z)$  K, by

$$v_{\text{th}} = 150(1+z)(m_\nu/1 \text{ eV})^{-1} \text{ km s}^{-1}. \quad (1)$$

The transition occurs at

$$1 + z_{\text{tr}} = 2 \times 10^3 \left( \frac{m_\nu}{1 \text{ eV}} \right). \quad (2)$$

For masses smaller than  $\sim 0.6$  eV, the transition occurs well into the matter-dominated era and after recombination. Therefore, massive neutrinos affect the anisotropies of the CMB temperature only through the background evolution. However CMB data strongly constrain other cosmological parameters that are degenerate with the neutrino mass, and is thus invaluable to joint analyses. The result would slightly differ for non-degenerate masses, for the normal or inverted hierarchies, but at a negligible level for a total mass above 0.2 eV (Lesgourgues et al. 2004).

After the transition, neutrino-density perturbations evolve in a similar way to CDM on scales larger than a free-streaming length, and are damped on smaller scales. The comoving free-streaming length is defined analogously to a Jeans length, by replacing the sound of speed by  $v_{\text{th}}$ , i.e.,  $\lambda_{\text{fs}}(t) = 2\pi \sqrt{2/3} v_{\text{th}}(t)/[a(t)H(t)]$ . It decreases from the time of transition onwards as,

$$\lambda_{\text{fs}} = 2\pi \times 1.2(1+z)^{1/2} (m_\nu/1 \text{ eV})^{-1} (\Omega_m h^2)^{-1/2} \text{ Mpc}, \quad (3)$$

which is valid at high redshift. The maximum occurs at the transition and is given by,

$$\lambda_{\text{fs}}^* = 2\pi \times 55 (\Omega_m h^2)^{-1/2} \left( \frac{m_\nu}{1 \text{ eV}} \right)^{-1/2} h^{-1} \text{ Mpc}. \quad (4)$$

The density perturbations of the other components, in particular CDM, are affected by the presence of massive neutrinos as a consequence of the change in the background evolution, the change in the time of equality, and feedback from the neutrino perturbations. Roughly speaking, the effect of  $m_\nu = 1$  eV neutrinos in the power spectrum is similar to the CDM effect on large scales  $k = 2\pi/\lambda < k_{\text{fs}}(z_{\text{tr}}) \approx 0.01 \text{ Mpc}^{-1}$ ; a scale-dependent suppression of the power spectrum amplitude at intermediate scales  $0.01 \text{ Mpc}^{-1} \lesssim k < k_{\text{fs}}(z=0) \approx 0.5 \text{ Mpc}^{-1}$ ; and a scale-independent suppression of amplitude at small scales  $k \gtrsim 0.5 \text{ Mpc}^{-1}$ .

Various combinations of cosmological data have been used to constrain the neutrino mass. Using CMB data alone, the WMAP 5-year analysis obtained an upper 95% confidence limit on the sum of the neutrinos masses of 1.3 eV, for a  $\Lambda$ CDM cosmology (Komatsu et al. 2009). By adding galaxy clustering data to CMB data and marginalizing over the galactic bias, the upper limit decreases to around 0.7 eV–1.0 eV, depending on the datasets used (e.g., Tegmark et al. 2006; Fogli et al. 2008). If instead, distance indicators (supernovae and baryon acoustic oscillations) were combined with CMB, stronger constraints were obtained, e.g.,  $\sum m_\nu < 0.61$  eV (Komatsu et al. 2009). When all of these probes were used together, the result improved to around 0.4 eV–0.5 eV (e.g., Goobar et al. 2006; Kristiansen et al. 2007). Similar results were obtained using only CMB and galaxy clustering data but assuming that the bias was known

(McTavish et al. 2006), or measuring it independently (Seljak et al. 2005). By applying the latter technique to WMAP 5-year data and new galactic bias constraints, an improved value of  $\sum m_\nu < 0.28$  eV was obtained (De Bernardis et al. 2008). Lyman- $\alpha$  data was also added to different combinations of probes, producing results of around 0.15 eV–0.3 eV, including the tightest constraint to date of  $\sum m_\nu < 0.17$  eV (Seljak et al. 2006).

In this paper we present the first constraints on neutrino masses obtained with cosmic shear data. The possibility of using the effect of weak gravitational lensing of background galaxies by large-scale structures, or cosmic shear (see Munshi et al. 2008, for a review), to constrain neutrino properties was first studied in Cooray (1999). Since then, various forecasts have been made and future cosmic shear surveys in combinations with redshift information and CMB data from Planck are expected to measure the sum of neutrino masses with an accuracy of  $\sim 0.05$  eV, using shear tomography (Hannestad et al. 2006) or the full 3D shear field (Kitching et al. 2008). In the present work, we use the latest release of the CFHTLS wide survey, CFHTLS-T0003, where two-point angular correlations of the cosmic shear field were detected on scales ranging from  $1'$  to  $4^\circ$  (Fu et al. 2008). The signal was measured on source galaxies with mean redshift  $z_m = 0.92$ , implying it is produced mainly by the dark matter distribution at  $z \approx 0.4$ . The measured range therefore probes the non-linear matter power spectrum on comoving scales of  $0.08 < k < 10 h \text{ Mpc}^{-1}$ , reaching the quasi-linear regime of largest scale corresponding to a physical size of approximately  $1 h^{-1} \text{ Gpc}$ . This largest scale probed is still one order of magnitude smaller than the largest free-streaming scale,  $k_{\text{fs}}^* \approx 0.01 \text{ Mpc}^{-1}$ , computed from Eq. (4). The data probes thus both the scale-independent and the scale-dependent suppression effects of the sub-free-streaming regime.

We proceed by presenting in Sect. 2 the methodology followed to compute the spectra. In the same section we introduce the statistical analysis performed and the datasets used. Cosmological constraints are obtained and discussed in Sect. 3 and our conclusions are presented in Sect. 4.

## 2. Methodology

### 2.1. Implementing massive neutrinos in cosmic-shear 2-point correlation functions

We perform a statistical analysis of a mixed dark-matter scenario by considering a 8+1 dimensional parameter space (see Sect. 2.2). For each sampled model of this parameter space the cosmic-shear power spectrum  $P_\gamma(\ell)$  is computed by integrating the non-linear total matter power spectrum  $P_m^{\text{nl}}$  along the line-of-sight, up to the limiting redshift of the survey  $z_{\text{lim}}$ , to account for the distribution of source galaxies  $n(z)$ . It is given by

$$P_\gamma(\ell) = \frac{9\Omega_m^2 H_0^4}{4c^4} \int_0^{z_{\text{lim}}} \frac{dz}{H(z)} (1+z)^2 W^2(z) P_m^{\text{nl}}(k, z), \quad (5)$$

where  $k = \ell/S_K(\chi(z))$  and

$$W(z) = \int_z^{z_{\text{lim}}} dz' n(z') \frac{S_K[\chi(z') - \chi(z)]}{S_K[\chi(z')]} \quad (6)$$

defines the lensing efficiency window function, and  $S_K[\chi(z)]$  denotes the comoving angular diameter distance as function of redshift, which reduces to the comoving radial distance  $\chi(z)$  for spatial flatness  $K = 0$ . The redshift distribution of sources was

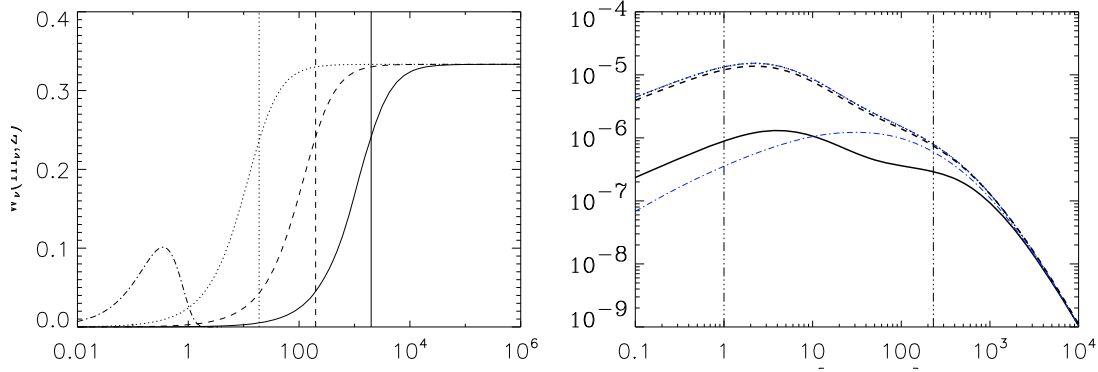


**Fig. 1.** *Left:* equation-of-state of fermionic massive particles as function of redshift  $z$  for  $m = 1.0$  eV (solid line),  $0.1$  eV (dashed) and  $0.01$  eV (dotted). The transition redshift, Eq. (2), is indicated in each case. The dashed-dotted curve shows the lensing efficiency window (arbitrary normalization). *Right:* aperture-mass variance  $\langle M_{\text{ap}}^2(\theta) \rangle$  with massive and massless neutrinos as function of angular scale. The massless neutrinos model (blue, thin lines) is shown in both linear and non-linear (HALOFIT) approximations. This indicates that the CFHTLS-T0003 data range (defined by the vertical lines) lies mostly in the non-linear regime, where the linear-approximation curve is much lower, and reaches the quasi-linear regime. Black, thick curves show three models of massive neutrinos (same masses and line types as in the left panel) with identical total mass densities ( $\Omega_{\text{m}} h^2 = 0.14$ ). The models for the two lighter neutrino cases are indistinguishable, while the case  $m_{\nu} = 1.0$  eV produces a significantly lower signal at small scales.

determined in Fu et al. (2008) from the photometric redshift estimations of Ilbert et al. (2006). We adopt the commonly used fitting function of

$$n(z) = N(z/z_s)^\alpha \exp\left[-(z/z_s)^\beta\right] \quad (7)$$

with best-fit parameters  $\alpha = 1.47$ ,  $\beta = 2.15$ , and  $z_s = 0.90$ , and a normalization constant  $N$  that was determined by integrating up to  $z_{\text{lim}} \simeq 6$ .

The shear power spectrum is integrated over the appropriate window function to obtain the mass variance in apertures  $\theta$  (Schneider et al. 1998),

$$\langle M_{\text{ap}}^2(\theta) \rangle = \frac{288}{\pi\theta^4} \int \frac{d\ell}{\ell^3} J_4^2(\ell\theta) P_\gamma(\ell), \quad (8)$$

where  $J_4$  is the 4th-order Bessel function of the first kind.

All quantities relying on the background evolution depend on the equation-of-state of the various matter components. The neutrino equation-of-state is defined as  $w_\nu(m_\nu, z) = P(m_\nu, T(z))/\rho(m_\nu, T(z))$ . We compute the pressure  $P$  and the energy density  $\rho$  at points of a grid  $(m_\nu, T(z))$ , using the fact that the distribution of neutrinos in the phase space is a Fermi-Dirac distribution. The result is well approximated by the fitting function

$$w_\nu(m_\nu, z) = \frac{1}{3} \left[ 1 + \left( \frac{m_\nu}{(1+z)0.058 \text{ eV}} \right)^a \right]^{-b}, \quad (9)$$

where  $a = 1.652$  and  $b = 0.561$ , and is shown in Fig. 1 (left panel). The transition to the non-relativistic regime occurs earlier for heavier particles, at the redshift given by Eq. (2) and indicated in the figure. The lensing efficiency window shows the redshift range probed by our data. At the upper end of this range,  $w_\nu$  is far from zero, especially for low masses. There is thus a degeneracy between the characteristic redshift of the sources and the neutrino mass, which is independent of the well-known redshift-mass degeneracy defined by the amplitude of the cosmic shear signal.

The total matter power spectrum in Eq. (5) is computed following Hannestad et al. (2006), which is also similar to the description adopted for perturbed quintessence fields

(Schimd et al. 2005). By assuming that the neutrino overdensities remain always in the linear regime while CDM and baryons grow non-linearly, the total matter power spectrum is given by

$$P_{\text{m}}^{\text{nl}}(k, z) = \left[ f_\nu \sqrt{P_\nu^{\text{lin}}(k, z)} + (f_{\text{cdm}} + f_{\text{b}}) \sqrt{P_{\text{cdm+b}}^{\text{nl}}(k, z)} \right]^2, \quad (10)$$

where  $f_i \equiv \Omega_i/\Omega_{\text{m}}$  with  $i = \{\nu, \text{cdm}, \text{b}\}$  are the density fractions of each matter field over the total matter density parameter  $\Omega_{\text{m}} = \Omega_{\text{cdm}} + \Omega_{\text{b}} + \Omega_\nu$ . The linear power spectra  $P_i^{\text{lin}}(k, z)$  are computed using the Boltzmann code CAMB<sup>1</sup>, to take into account properly the scale-dependent growth of the neutrino perturbations. The output is computed for a grid of redshifts linearly spanning the range  $0 < z \leq 4$  and then spline-interpolated. The non-linear spectrum  $P_{\text{cdm+b}}^{\text{nl}}$  is computed with the HALOFIT mapping (Smith et al. 2003). The Peacock & Dodds mapping (Peacock & Dodds 1996) is unsuitable for this study, because it uses a scale-independent growth factor, which cannot be defined in the presence of neutrinos.

The right panel of Fig. 1 shows the aperture mass dispersion in the presence of massive and massless neutrinos, computed from the total matter power spectrum, for the same  $\Omega_{\text{m}}$ . The models are similar on large scales where the neutrinos behave like cold dark matter and show a scale-dependent deviation on intermediate scales. On small scales, which stay always inside the free-streaming length, the suppression is constant. Linear perturbation theory predicts the small-scale suppression to be,  $[P_{\text{m}}^{\text{lin}}(f_\nu, z=0) - P_{\text{m}}^{\text{lin}}(f_\nu=0, z=0)]/P_{\text{m}}^{\text{lin}}(f_\nu, z=0) \sim -8f_\nu$  (Hu et al. 1998). For the non-linear power spectrum, the suppression is higher, around  $-10f_\nu$ , as predicted by both numerical simulations (Brandbyge et al. 2008) and one-loop corrections (Wong 2008). For the aperture mass dispersion, the models shown in Fig. 1 have a small-scale suppression of  $\sim -5f_\nu$ .

## 2.2. Likelihood analysis

### 2.2.1. Cosmic shear alone

The statistical analysis evaluates a mixed dark matter scenario with nine parameters, including the reduced Hubble parameter  $h$ , the density of baryons  $\omega_{\text{b}} \equiv \Omega_{\text{b}} h^2$ , cold dark matter,

<sup>1</sup> <http://camb.info>

$\omega_{\text{cdm}} \equiv \Omega_{\text{cdm}} h^2$ , and massive neutrinos,  $\omega_\nu \equiv \Omega_\nu h^2$ , the effective number of relativistic degrees of freedom  $N_{\text{eff}}$ , the optical depth to reionization  $\tau$ , the primordial spectral index  $n_s$ , the rms of the matter perturbations extrapolated to redshift  $z = 0$  and filtered over the  $8h^{-1}$  Mpc scale,  $\sigma_8$ , and the mean redshift  $z_m$  of the source galaxies. The results will be marginalized over a mean redshift range  $0.78 < z_m < 1.0$ , corresponding to the  $2\sigma$  interval of the redshift distribution found in Fu et al. (2008). The neutrino physical density parameter relates to the total neutrino mass as  $\Omega_\nu h^2 = \sum m_\nu / 93$  eV, and we assume that the three neutrino masses are degenerate.

In a very conservative approach, we shall work in a Friedmann-Lemaître-Robertson-Walker (FLRW) cosmology with cosmological constant as dark energy, with energy density fixed assuming spatial flatness. More generally, in this framework, dark energy is a fluid-like component that is dominant at low redshift and responsible for the recent accelerated expansion. A quintessence field, eventually allowing for non-minimal couplings (Wetterich 1995; Uzan 1999; Tocchini-Valentini & Amendola 2002), provides the most general alternative that might alleviate the coincidence problem (e.g., Copeland et al. 2006, for a review). Alternatively, it is possible to account for the global dynamics without advocating such an additional field, by considering back-reaction effects of structure formation (Ellis & Buchert 2005; Kolb et al. 2006; Wiltshire 2007), rejecting the Copernican principle (Uzan et al. 2008), or invoking theories of gravitation that differ from general relativity on large scales (see Uzan 2006, for a review). Our results do not exclude these possibilities, which require new, consistent analyses to be evaluated properly (see e.g., Schmid et al. 2007, for a weak-lensing analysis of quintessence).

The log-likelihood is defined as usual to be

$$\log \mathcal{L} = -\frac{1}{2} \sum_{ij} \Delta \langle M_{\text{ap}}^2(\theta_i) \rangle (\text{Cov}^{-1})_{ij} \Delta \langle M_{\text{ap}}^2(\theta_j) \rangle, \quad (11)$$

where  $\Delta \langle M_{\text{ap}}^2(\theta_i) \rangle$  is the difference between the observed and the theoretical values of the aperture mass variance computed at angles  $1' \leq \theta_i \leq 230'$  and  $\text{Cov}$  is the corresponding covariance matrix.

We sample the likelihood over a regular grid of the parameter space, for a total of  $\sim 10^7$  models. The domain of the grid is:  $\omega_b \in [0.0186, 0.0249]$ ,  $\omega_{\text{cdm}} \in [0.110, 0.152]$ ,  $\omega_\nu \in [0, 0.042]$ ,  $h \in [0.62, 0.80]$ ,  $N_{\text{eff}} \in [2, 4]$ ,  $\tau \in [0, 0.225]$ ,  $n_s \in [0.87, 1.02]$ ,  $\sigma_8 \in [0.65, 0.92]$ .

In this work we use the aperture mass vector and covariance matrix obtained in Fu et al. (2008), which was measured over 57 square degrees (35 square degrees of effective area) in three connected patches of the sky, using  $2.5 \times 10^6$  galaxies with magnitudes  $21.5 < i_{\text{AB}} < 24.5$ . The covariance matrix includes shape noise in the shear estimator, non-Gaussian cosmic variance, and the residual B-mode. The shear-measurement pipeline was tested on STEP2 simulations (Massey et al. 2007) and shown to be slightly biased, underestimating the shear on average by 2% (Fu et al. 2008). Moreover, this analysis showed that highly anisotropic point-spread-functions (PSF) may introduce a spurious constant shear. The aperture mass statistic, being computed with a compensated filter, is unaffected by a constant shear, which is the main reason for choosing this statistic for the present analysis. In contrast, a constant shear affects top-hat two-point statistics. The impact of redshift-dependent additive and multiplicative shear biases, which are present in all KSB-based shear estimators, on cosmological constraints is studied in Semboloni et al. (2008).

## 2.2.2. Joint analysis

In the joint analysis, we adopt the *importance sampling* technique (Hastings 1970; Lewis & Bridle 2002), adding CFHTLS-T0003 cosmic shear data to two Monte Carlo Markov chains available in the LAMBDA archive<sup>2</sup> for the mixed dark-matter scenario. One of the chains was computed for CMB temperature and polarization anisotropies derived from WMAP-5yr (Dunkley et al. 2009) data. The other chain used a combination of these data with baryon acoustic oscillations from SDSS and 2dFGRS (Percival et al. 2007), and type Ia supernovae from the ‘‘Gold’’ sample (Riess et al. 2004) and SNLS (Astier et al. 2006).

Importance sampling consists of estimating a target distribution (a joint posterior distribution in our case) by sampling an auxiliary distribution. We assume that the public Monte Carlo Markov chains provided by the WMAP team have enough resolution at the region of parameter space intersecting the cosmic shear posterior distribution. This is a reasonable assumption since they are the dominant contribution to the joint constraints. They are thus useful auxiliary distributions and are biased distributions of the target distributions. To obtain the two unbiased joint distributions (WMAP+CFHTLS and WMAP+BAO+SNe+CFHTLS), we scale the chains by multiplying the weight of each chain element by its likelihood with respect to the cosmic shear data.

This method allows us to accelerate the computation compared to sampling directly the joint posterior with a grid or a Markov chain, since it requires only the computation of the cosmic shear likelihood for each model of the chains. Each model of the chains has a constant  $N_{\text{eff}} = 3.04$ , hence in the joint analysis, we consider only 7+1 physically independent parameters, i.e., the remaining 7 cosmological parameters used in the cosmic shear analysis and the lensing sources redshift.

## 3. Results

### 3.1. CFHTLS-T0003 alone

We now discuss the analysis of cosmic-shear data alone. Figure 2 shows the marginalized confidence contours in the  $(\sigma_8, \Omega_m)$  plane. The degeneracy direction in the case of massless neutrinos is fitted by

$$\sigma_8 (\Omega_m / 0.25)^{0.72} = 0.744 \pm 0.052. \quad (12)$$

This value was found by marginalizing over  $h$  but for fixed  $\omega_b$  and  $n_s$  to be more directly comparable to the result of Fu et al. (2008) for the same data. Our result is slightly lower, but within  $1\sigma$ . There are several differences between the two analyses that account for this difference. In particular, since we are interested in combining our results with CMB constraints, we explored a narrower grid in  $(\omega_b, \omega_{\text{cdm}}, \omega_\nu)$ , corresponding to a grid interval of  $\Omega_m \in [0.2, 0.6]$ . The boundary effects slightly increase the curvature of the contour, which is most accurately described with a larger exponent power-law. The comparison of both results is particularly sensitive to this choice because here the confidence intervals are computed as volumes of the posterior distribution containing a certain fraction of the total probability, whereas in Fu et al. (2008) the results are obtained from the values of  $\Delta\chi^2$ . The theoretical modelling also differs. Here we use Eq. (10), while in Fu et al. (2008) the power spectrum was computed from the Eisenstein & Hu transfer function (Eisenstein & Hu 1998).

<sup>2</sup> <http://lambda.gsfc.nasa.gov/>

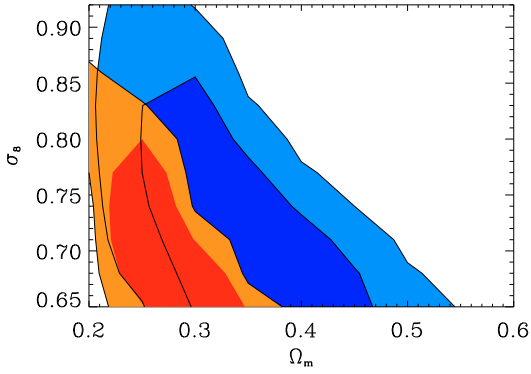


**Fig. 2.** Confidence contours (68% and 95%) from the aperture-mass dispersion between  $1'$  and  $230'$ , for  $\Omega_\nu = 0$  (red, smaller) and marginalized over  $\omega_\nu$  (blue, larger). Both cases are marginalized over the source redshift distribution and the remaining cosmological parameters.

In the presence of massive neutrinos, the contours are shifted towards the right. This follows from the  $\Omega_{\text{cdm}} - \Omega_\nu$  degeneracy, and shows that an increase in  $\Omega_\nu$  is compensated by an increase in  $\Omega_{\text{cdm}}$ , confirming that the data are in the sub-free-streaming-length regime, where the effect of the neutrinos opposes that of the cold dark matter. The contours also broaden, since many more preferred models exist now. For example, on angular scales of between  $10'$  and  $100'$ ,  $\langle M_{\text{ap}}^2(\theta) \rangle$  of the best-fit models of the full grid and the massless neutrino sub-grid, differ by less than 5%. As the contours broaden, their shape remains unchanged, implying that the CDM effect on the cosmic shear signal is more significant than that of the neutrinos. The degeneracy direction in the case of massive neutrinos is now fitted by

$$\sigma_8 (\Omega_m/0.35)^{0.64} = 0.711 \pm 0.076, \quad (13)$$

where we chose a higher pivot  $\Omega_m$ .

Figure 3 (left panel) shows the massless and massive neutrino best-fit models, ( $m_\nu = 0$  eV,  $\Omega_m = 0.30$ ) and ( $m_\nu = 0.53$  eV,  $\Omega_m = 0.44$ ), respectively. They have the same values of  $\sigma_8$  and  $h$  and differ in  $n_s$ . The difference between the two models, shown in the inset normalized by the massless neutrino model, increases on larger scales with the approach to the free-streaming-length. This indicates that combining cosmic shear measurements at sub- and super-free-streaming-scales, might break the  $\Omega_{\text{cdm}} - \Omega_\nu$  degeneracy. Shown explicitly in Fig. 3 (middle panel), this degeneracy, as well as the similarly-oriented  $\sigma_8 - \Omega_\nu$  correlation (not shown), confirm that an increasing neutrino density decreases the cosmic shear signal. However, the tilting effect of the neutrino density on the matter power spectrum around the free-streaming scale may mimic the dependence on  $n_s$ , especially if the pivot scale  $k$  used is similar to the free-streaming scale  $k_{\text{fs}}^* \sim 0.01h \text{ Mpc}^{-1}$ . Therefore, the combination of sub- and super-free-streaming data may not have enough information to additionally break the  $n_s - \Omega_\nu$  degeneracy. This degeneracy is shown in the right panel of Fig. 3.

To explore the benefit of a broader range of scales, we construct a fiducial model consisting of an extension of our best-fit massless neutrino model to  $\theta = 20^\circ$  (also shown in Fig. 3, left panel), where the flat-sky approximation remains valid. We computed a new covariance matrix using the Schneider et al. (2002) approximation with the Semboloni et al. (2007) non-Gaussian correction and WMAP-5yr mean parameter values (Dunkley et al. 2009). We assumed the same sky coverage and galaxy density as in CFHTLS-T0003. In this way we can evaluate the benefit of using large scales independent of a gain due to better

statistics. We obtain constraints similar to the ones obtained for the data up to  $230'$ , the extension to  $\theta = 20^\circ$  only adding a small number of independent points. Since the cosmic shear signal on large scales becomes very small, better statistics are needed in attempting to break the  $\Omega_{\text{cdm}} - \Omega_\nu$  degeneracy with cosmic shear data alone.

Using either CFHTLS-T0003 data or its extension to  $\theta = 20^\circ$ , the marginalized upper bound on the neutrino mass is,

$$\sum m_\nu < 3.3 \text{ eV (95% C.L.)}. \quad (14)$$

This constraint, while very loose when compared with the combined constraints mentioned in Sect. 2, is comparable to the ones obtained from SDSS or 2dF galaxy redshift surveys alone (see e.g., Kristiansen et al. 2007, who find  $\sum m_\nu \lesssim 5.2$  eV).

We note that the 95% C.L. contours in Fig. 2 do not close inside the range of the parameters probed. This implies that our grid limits are an effectively strong prior, in particular implying  $\Omega_m \in [0.2, 0.6]$  and  $\sigma_8 \in [0.65, 0.92]$ . In other words, the constraint in Eq. (14) includes a marginalisation over an arbitrary and relatively narrow range of parameters values, and is thus optimistic. Furthermore, the derived constraint does not take account of degeneracies with dark energy. In more general scenarios with non-vanishing curvature or with non-cosmological-constant dark energy, both growth of structure and distances, as functions of redshift, depend on both the dark-energy density parameter  $\Omega_{\text{de}}$  and the equation-of-state  $w_{\text{de}}$ . To effectively break the  $\Omega_\nu - \Omega_m$  degeneracy, it will thus be necessary to use a measure that is not degenerate in  $\Omega_{\text{de}}$  and  $w_{\text{de}}$ . One possibility is to exploit the lens efficiency at different redshift bins with tomography (e.g., Abazajian & Dodelson 2003). However, even with tomography, some direct neutrino-dark energy degeneracy will remain due to the transition epoch from matter to dark-energy domination (Kia Kotou et al. 2008).

Regarding the effective number of relativistic species, cosmic shear is sensitive to it via the change in the matter-radiation equality. A higher  $N_{\text{eff}}$  implies a longer radiation-dominated era, and thus a more efficient suppression of growth. Hence, the relative amplitude of small and large scales changes and the shear power spectrum tilts. The effect is however weak and we find an essentially flat likelihood in the probed range of  $N_{\text{eff}} \in [2, 4]$ , meaning that the data do not constrain this parameter.

### 3.2. Joint analysis

We now explore the parameter space by adding CFHTLS-T0003 cosmic shear data to each of the Monte Carlo Markov chains defined in Sect. 2.2.2, aiming to determine the gain achieved by including lensing data.

The main independent piece of information provided by cosmic shear is the power spectrum on small scales. As discussed above, it has a distinctive scaling with both neutrino and CDM densities, while these two parameters for CMB are instead weakly correlated, as seen in Fig. 4 (left panel, largest contour). This allows us to obtain a narrow, joint constraint, approximately in the same direction found for cosmic shear alone in Fig. 3 (middle panel). The direction orthogonal to the contour indicates the combination of parameters to which cosmic shear is mostly sensitive to. It is well approximated by the linear relation  $\omega_{\text{cdm}} - \omega_\nu$  and the WMAP5 + CFHTLS constraint on this combination of parameters is,

$$\omega_{\text{cdm}} - \omega_\nu = 0.106 \pm 0.006 (1\sigma). \quad (15)$$

The figure-of-merit (FoM) quantifies the error ellipses of correlated parameters and was introduced for the parameters of the

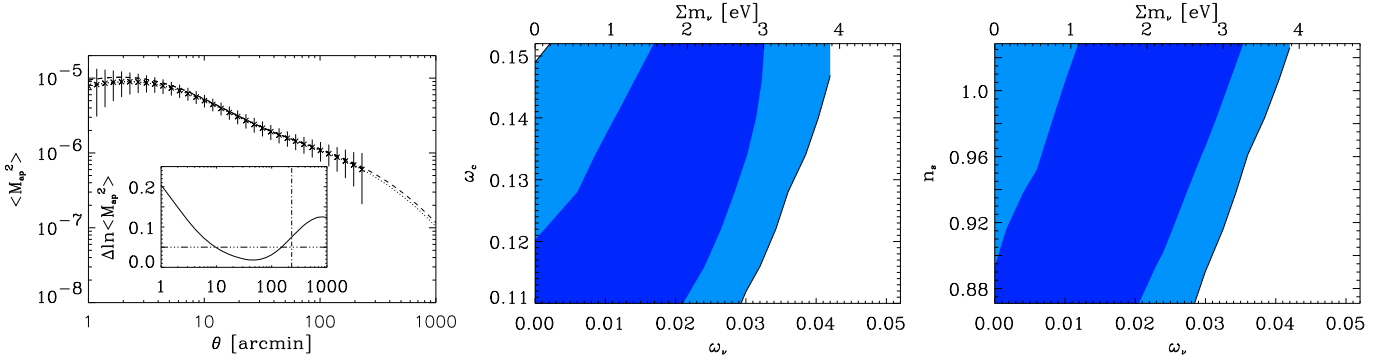


**Fig. 3.** *Left:* best-fit models found for massive ( $m_\nu = 0.53$  eV,  $\Omega_m = 0.44$ ; dashed) and massless ( $m_\nu = 0$  eV,  $\Omega_m = 0.30$ ; dotted) neutrino cases. Error bars are from CFHTLS-T0003. The models are extended beyond the data limit to illustrate the model separation at large scales. The normalized difference between the models is shown in the inset, where the horizontal line marks a 5% model-separation and the vertical line shows the data limit. *Middle and right:* confidence contours (68% and 95%) from the aperture-mass variance, in the  $(\omega_\nu, \omega_{\text{cdm}})$  and  $(\omega_\nu, n_s)$  planes, marginalized over the hidden parameters.

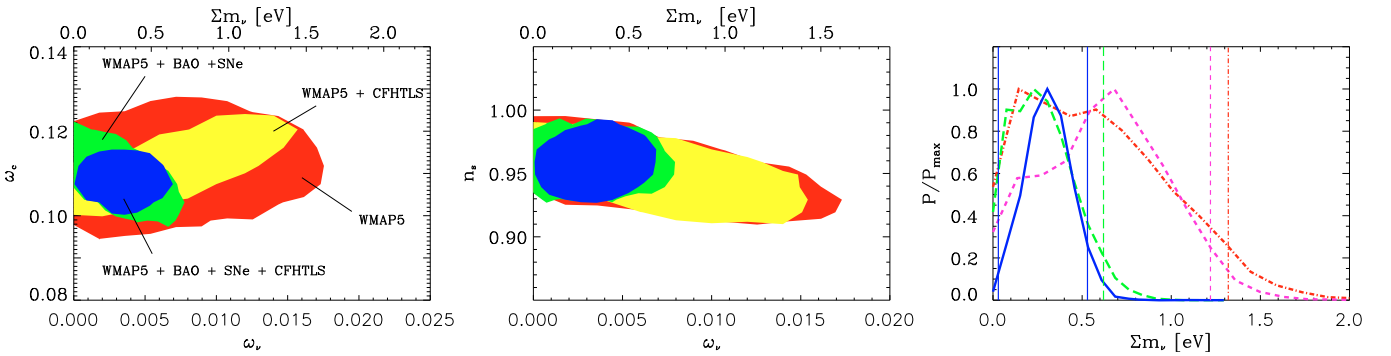


**Fig. 4.** *Joint analysis. Left and middle:* contours at 95% C.L. of  $(\omega_\nu, \omega_{\text{cdm}})$  and  $(\omega_\nu, n_s)$  for the four cases considered: WMAP5 alone (largest contour, red), WMAP5+CFHTLS (second largest, yellow), WMAP5+BAO+SNe (second smallest, green), WMAP5+BAO+SNe+CFHTLS (smallest contour, blue). *Right:* one-dimensional marginals for  $\Sigma m_\nu$  showing the 95% C.L. with vertical lines, for the same four cases: WMAP5 (dash-dot, red); WMAP5+CFHTLS (dash, pink); WMAP5+BAO+SNe (long dash, green); and WMAP5+BAO+SNe+CFHTLS (solid, blue). For the latter a lower bound was also found).

dark energy equation of state (Albrecht et al. 2006). It is defined as the inverse area of the ellipse approximating the  $p\%$  confidence level contour, centered on the contour centroid, i.e.,

$$\text{FoM}^{-1} = \Delta\chi^2(p)\pi (\sigma_{11}\sigma_{22} - \sigma_{12}^2)^{1/2}, \quad (16)$$

where  $\sigma_{ii}$  is the variance of the parameter  $i$ . We consider  $2\sigma$  contours, for which  $\Delta\chi^2(95.4\%) = 6.17$ , and obtain  $\text{FoM} \simeq 19$  for the WMAP5 contour and  $\text{FoM} \simeq 44$  for the combined (WMAP5 + CFHTLS) case, corresponding to a gain of a factor of 2.3. The two parameters  $\omega_{\text{cdm}}$  and  $\omega_\nu$  are, however, strongly correlated, exhibiting a narrow, long combined contour and the effective gain in the  $\omega_\nu$  variance is of only 1.2.

The introduction of distance measurements (BAO+SNe) is useful, since its combination with WMAP5 data (also shown in Fig. 4, left panel) defines a narrow region in the  $(\omega_{\text{cdm}}, \omega_\nu)$  plane that complements that of the WMAP5+CFHTLS data. Both cases thus probe orthogonal combinations of the two parameters and, furthermore, in a way that is independent of the spectral index, since this is already well determined by the CMB data alone (as shown in Fig. 4, middle panel). Their combination thus has the same properties we were looking for when discussing the possibility of using sub- and super-free-streaming scales from cosmic shear alone, along with the need for an independent measure of  $n_s$ . This means that the combination of the two cases (WMAP5 + BAO + SNe + CFHTLS) breaks the remaining degeneracy, as is clear from Fig. 4 (left panel, smaller

contour) and from the fact that the combined contour has very small correlation ( $\sigma_{12} < 0.1\%$ , for un-normalised parameters  $\omega_c$  and  $\omega_\nu$ ).

Figure 4 (right panel) shows the one-dimensional marginalized probability distributions of the neutrino masses in the four cases. The upper 95% confidence levels are  $\Sigma m_\nu < 1.32$  eV (WMAP5),  $\Sigma m_\nu < 1.22$  eV (WMAP5 + CFHTLS) and  $\Sigma m_\nu < 0.62$  eV (WMAP5 + BAO + SNe). For the full combination (WMAP5 + BAO + SNe + CFHTLS), we find that

$$0.03 \text{ eV} < \Sigma m_\nu < 0.54 \text{ eV} \quad (95\% \text{ C.L.}), \quad (17)$$

with mean 0.31 eV. Interestingly, we obtain a lower bound, and thus a preference for massive neutrinos at the  $2\sigma$  level.

It is worth to point out that the lower bound on  $\Sigma m_\nu$  is strongly dependent on the position of the WMAP5 + CFHTLS contour in the  $(\omega_\nu, \omega_{\text{cdm}})$  plane (see Fig. 4, left panel). Any systematic effect that underestimates the cosmic-shear signal would shift the  $(\Omega_m, \sigma_8)$  contour towards the bottom-left corner of Fig. 2 with a consequent shift in the  $(\omega_\nu, \omega_{\text{cdm}})$  contour towards the bottom-right corner of Fig. 4 (left panel). The WMAP5 + BAO + SNe + CFHTLS contour would thus descend along the WMAP5 + BAO + SNe one producing a positive lower bound for the neutrino mass. A similar effect appeared in Allen et al. (2003), which also showed a preference for a non-zero neutrino mass from a combination of CMB, galaxy clustering and X-ray cluster data; that result was in fact caused by an underestimation of  $\sigma_8$ , as pointed out by Seljak et al. (2005). Similarly,

the joint constraint depends crucially on BAO data. Komatsu et al. (2009) pointed out a tension between SNe and BAO results when the joint SDSS + 2dFGRS BAO sample is used. If BAO data overestimates the total matter density, then an unbiased WMAP5 + BAO + SNe contour in the  $(\omega_\nu, \omega_{\text{cdm}})$  plane (Fig. 4, left panel) will be shifted towards the bottom-left corner, weakening the preference for massive neutrinos.

### 3.3. Robustness of the constraints

We check here the robustness of our results against systematics of the cosmic shear data, that have not been included in the analysis so far. For this purpose, we first assume the data vector is biased as a consequence of an underestimation in the shear, as indicated by the STEP simulations. We assume a 2% redshift-independent bias in the shape measurements, which translates into a scale-independent 4% error in the data vector, and repeat the joint analysis. The resulting combined contour shifts upwards along the WMAP5+BAO+SNe degeneracy in agreement with the discussion in Sect. 3.2. As seen in Fig. 5 (left panel, solid lines), this small bias is enough for the evidence of massless neutrinos to be lost and we obtain at the 95% C.L.:

$$\sum m_\nu < 0.53 \text{ eV}. \quad (18)$$

Other sources of errors that can affect cosmic-shear cosmological constraints are: contamination from intrinsic alignments, in particular shear-shape correlations (Hirata & Seljak 2004) for no precise theoretical modeling yet exists; uncertainties in the photometric redshifts; and extra PSF residuals not predicted by the STEP simulations. Modelling of some of the CFHTLS-T0003 systematics is included in the analysis of Kilbinger et al. (2009). Here we consider the rougher approach of marginalizing over a scale-independent calibration factor, accounting for all possible sources of biases, with the goal of finding a threshold of contamination above which the CFHTLS data do not improve the combined constraints.

We find a threshold of 25% for the aperture mass dispersion data. The corresponding combined contour in the  $(\omega_\nu, \omega_{\text{cdm}})$  plane is shown in Fig. 5 (left panel, dashed lines). The contour is now elongated and similar to the WMAP+BAO+SNe one of Fig. 4 (left panel). If the data contains systematics of amplitude smaller than 25% of the signal, we can quote conservative combined constraints by marginalizing over the amplitude of the systematics. The final 95% C.L. for the joint analysis will be intermediate between the most optimistic case (no bias) of  $0.03 \text{ eV} < \sum m_\nu < 0.54 \text{ eV}$  and the worst case (no contribution from lensing) of  $\sum m_\nu < 0.62 \text{ eV}$ . For example, in the case of systematics of 10%, the conservative constraints are  $\sum m_\nu < 0.58 \text{ eV}$ . These marginalized constraints, not including systematics with a scale- or a redshift-dependence, are approximative since massive neutrinos affect both the amplitude and the shape of the cosmic shear correlations. Only on smaller scales ( $\lesssim 10'$ , see e.g. Fig. 1 right panel) is the suppression scale-independent.

We can also assess the robustness of the result by comparing it with a forecast. For this, we compute a systematics-free cosmic-shear covariance matrix for our survey size using the results of Schneider et al. (2002) and Semboloni et al. (2007). This covariance matrix differs from the one we have used so far, which was computed by taking into account the true galaxy positions and weights. The results do not change when we replace the covariance matrices, as shown in Fig. 5 (middle and right panels, solid lines). To ensure that the forecast is completely independent of the data, we redo it by further replacing the data

vector by a fiducial model (the WMAP5 mean, Dunkley et al. 2009). This time we obtain a shift in the contour location (Fig. 5, middle and right panels, dashed lines). Again the evidence for massless neutrinos is lost, this time due to the higher  $\omega_{\text{cdm}}$  value of the WMAP5 fiducial model. This behaviour mimicks a correction for an eventual overestimation of the source redshifts. Indeed, if the effective redshift is lower, the models will have a higher value of  $\Omega_m$  for the same amplitude  $\sigma_8$ , shifting the combined  $\omega_{\text{cdm}} - \omega_\nu$  contour up. It likewise mimicks a correction for an underestimation of the shear measurements. The combined constraint on the neutrino mass, when using the WMAP5 fiducial model, strengthens to  $\sum m_\nu < 0.44 \text{ eV}$ . We note this is also the result that would be obtained if the data were corrected for a negative calibration bias of 20%.

In summary, the possible systematics do not change the angle between the  $\omega_{\text{cdm}} - \omega_\nu$  degeneracy in the WMAP5 + CFHTLS and WMAP5 + BAO + SNe cases, only shift or broaden the combined contour position and size. Eventual corrections for an underestimation of the data vector or for an overestimation of the source redshifts would produce both a tighter upper bound and a looser lower bound on the neutrino mass.

The matter power spectrum also contributes as a source of uncertainties. The prescription used, Eq. (10), does not consider clustering of neutrinos on CDM structures, which occurs when the neutrino thermal velocity drops below the velocity dispersion,  $v$ , of forming clusters; for instance, it takes place at  $z \sim 2.3$  for  $v \sim 1000 \text{ km s}^{-1}$  and  $m_\nu \sim 0.5 \text{ eV}$ . The corresponding neutrino halo profile is flatter in the centre than a pure CDM Navarro-Frenk-White (Ringwald & Wong 2004). Including it in the 1-halo term of the halo model, Abazajian et al. (2005) showed that it decreases the non-linear matter power spectrum. Accordingly, in this work the term  $P_{\text{cdm+b}}^{\text{nl}}$  is expected to be overestimated by  $\sim 1\%$  on scales around  $k = 0.5 h \text{ Mpc}^{-1}$  for  $m_\nu \sim 0.5 \text{ eV}$ . Alternatively, results from perturbation theory with neutrinos (Wong 2008) also indicate an overestimation of the matter power spectrum, as already mentioned in Sect. 2.1.

The non-linear power spectrum is computed with the HALOFIT, which declares a 3% uncertainty on scales  $k < 10 h/\text{Mpc}$  at  $z < 3$  (Smith et al. 2003), which are thus of the same order as the supposed shear measurement bias. This uncertainty is effectively both redshift- and scale-independent over the data redshift and scale ranges. Marginalizing over a 5% uncertainty, the corresponding joint constraint is  $\sum m_\nu < 0.56 \text{ eV}$ . Furthermore, the HALOFIT does not take account of the effects of cooling baryons and hot intra-cluster baryons, which are degenerate with the neutrinos, affecting the power spectrum by a few percent on small scales (White 2005; Zhan & Knox 2004; Jing et al. 2006).

## 4. Conclusions

We have investigated the potential of cosmic shear to constrain the mass of neutrinos. In the sub-free-streaming regime, the constraining power originates, for a fixed density of baryons, in the tendency of relativistic (hot) dark matter particles to escape from collapsed regions. Therefore additional amounts of CDM are needed to produce the same cosmic-shear distortion, shifting the  $\Omega_m - \sigma_8$  degeneracy towards larger values of  $\Omega_m$  with respect to the analysis without massive neutrinos (Fig. 2), producing a  $\omega_{\text{cdm}} - \omega_\nu$  degeneracy favoring higher amounts of CDM for higher amounts of massive neutrinos (Fig. 3). The analysis of CFHTLS-T0003 data alone yields a loose constraint of  $\sum m_\nu < 3.3 \text{ eV}$  at the 95% C.L., for our particular choice of priors.

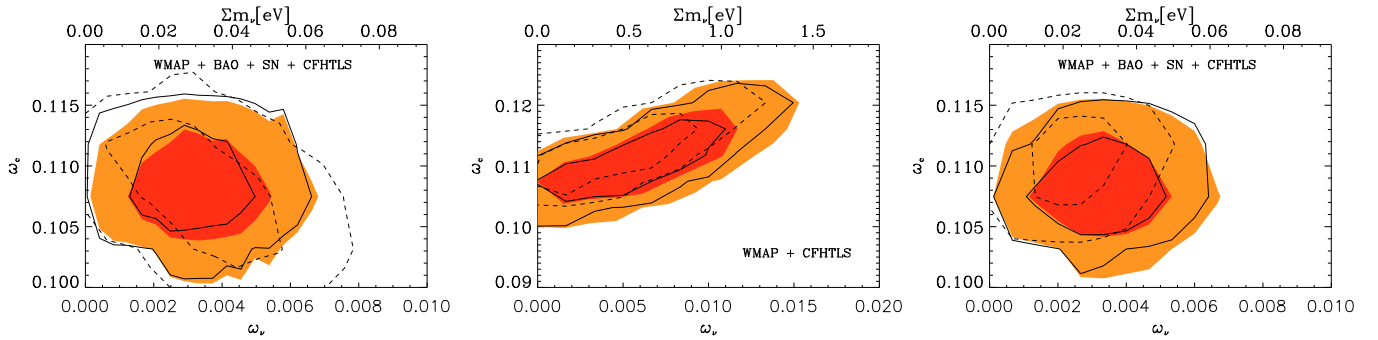


**Fig. 5.** Tests of the robustness of the result. Marginalized joint constraints (68% and 95% C.L.) obtained using the actual data (filled contours) and various assumptions (open contours). *Left:* impact of systematics, assuming a 4% underestimation (solid) or marginalizing over a  $\pm 25\%$  calibration bias (dashed). *Middle and right:* forecasts using a synthetic covariance matrix and the CFHTLS vector data (solid) or the same covariance matrix with a WMAP5 fiducial model (dashed).

We have explored larger angular scales using a synthetic data vector extended to  $20^\circ$  to explore the possibility of breaking the  $\omega_{\text{cdm}} - \omega_\nu$  degeneracy using only cosmic shear. This analysis did not predict an improvement in the results, which would require higher signal-to-noise ratio at large scales.

The introduction of CFHTLS-T0003 data in a WMAP5+BAO+SNe analysis provides an interesting combination, breaking the  $\omega_{\text{cdm}} - \omega_\nu$  degeneracy present in that analysis (Fig. 4, left panel). The joint analysis yields  $0.03 \text{ eV} < \sum m_\nu < 0.54 \text{ eV}$  at the 95% confidence level, marginally excluding massless neutrinos (Fig. 4, right panel). The preference for massive neutrinos is lost when the data is corrected for a possible underestimation of the shear signal, which simulations indicate may be around 4%. In this case, the result shifts to  $\sum m_\nu < 0.53 \text{ eV}$ . The CFHTLS data also shows some disagreement with the result of WMAP5. Indeed, if a cosmic-shear fiducial WMAP5 model was used, the expected combined WMAP5+BAO+SNe+CFHTLS constraint would be tighter:  $\sum m_\nu < 0.44 \text{ eV}$ . Finally, we showed that CFHTLS-T0003 data do not improve the WMAP5+BAO+SNe constraints on the neutrino mass if they contain a bias larger than 25%.

After submission of the manuscript, a similar study was submitted by Ichiki et al. (2009), also using CFHTLS-T0003 cosmic shear data to constrain the neutrino mass. Both analyses take a similar approach, the main differences being: they use the cosmic shear correlation function, which is more affected by systematics, as opposed to the aperture-mass dispersion; the non-Gaussian shear covariance matrix is also computed in different ways, as is the likelihood analysis. Their neutrino mass constraints from cosmic shear only are weaker, which is consistent with the fact they impose weaker priors, and the results for a WMAP5+BAO+SNe+CFHTLS joint analysis are very similar.

Besides the neutrino mass, we also considered the effective number of relativistic degrees of freedom,  $N_{\text{eff}}$ . CMB anisotropies are by far more sensitive than cosmic shear and CFHTLS-T0003 data produced an almost flat likelihood with respect to this parameter. This prevented us from using the  $\sigma_8 - N_{\text{eff}}$  degeneracy, caused by a higher  $N_{\text{eff}}$  delaying the matter-radiation equivalence and the corresponding defreezing of matter perturbations, which have less time to grow.

In summary, the CFHTLS cosmic-shear has already sufficient statistical precision for the accuracy of the results to be affected by systematics. The CFHTLS lensing systematics collaboration is currently undertaking a very detailed and lengthy analysis of those systematics. The statistical precision is however still insufficient to allow us to improve current constraints

on the neutrino mass. Future ground-based and space-borne observations (such as KIDS, Pan-STARRS, DES, LSST, SNAP-L, JDEM, or EUCLID surveys; see Peacock et al. 2006), with better statistics, larger scales, and also the use of tomographic techniques, will allow to perform more elaborate analyses, for instance enabling to relax the assumption of degeneracy between mass eigenstates.

From the theoretical point-of-view, a more suitable computation of the matter power spectrum in the non-linear regime will be mandatory, to take more careful account of the effects of massive neutrinos without relying on mappings based on  $\Lambda$ CDM  $N$ -body simulations. This might be achievable using either standard perturbation theory (e.g., Saito et al. 2008) or a resummation scheme (see e.g., Crocce & Scoccimarro 2006; Pietroni 2008). It will be interesting, eventually, to investigate the degeneracy with the low-redshift physics ( $z \lesssim 20$ ), such as reionization and dark energy, relevant if  $m_\nu \lesssim 0.01 \text{ eV}$ . On this mass scale, the normal/inverted hierarchy of mass states can also be distinguished. More elaborate models allowing for an interaction between massive neutrinos and a quintessence field (Brookfield et al. 2006), or in which mass-varying neutrinos behave as a negative pressure fluid, which could then be the origin of the cosmic acceleration (Fardon et al. 2004), may then also be considered.

*Acknowledgements.* We are thankful to Yannick Mellier for supporting this project and to Elisabetta Semboloni for many discussions. We thank Karim Benabed for help with computation in the early stage of this work and the Terapix group for computational facilities. We acknowledge the CFHTLS lensing systematics collaboration for helpful discussions. We are grateful to Peter Schneider and Jens Roediger for careful readings of the manuscript. We acknowledge use of CAMB and of the LAMBDA archive. IT and LF are supported by the European Commission Programme 6-th framework, Marie Curie Training and Research Network “DUEL”, contract number MRTN-CT-2006-036133. M.K. is funded by the CNRS/ANR research grant “ECOSSTAT”, contract number ANR-05-BLAN-0283-04. CS thanks IAP for hospitality.

## References

- Abazajian, K., & Dodelson, S. 2003, *Phys. Rev. Lett.*, 91, 041301
- Abazajian, K., Switzer, E. R., Dodelson, S., Heitmann, K., & Habib, S. 2005, *Phys. Rev. D* 71, 043507
- Albrecht, A., Bernstein, G., Cahn, R., et al. 2006 [arXiv:astro-ph/0609591]
- Allen, S. W., Schmidt, R. W., & Bridle, S. L. 2003, *MNRAS*, 346, 593
- Astier, P., Guy, J., Regnault, N., et al. 2006, *A&A*, 447, 31
- Bondi, F. 1960, *Cosmology* (Cambridge University Press)
- Brandbyge, J., Hannestad, S., Haugboelle, T., & Thomsen, B. 2008, *JCAP*, 08, 020B
- Brookfield, A. W., van de Bruck, C. Mota, D. F., & Tocchini-Valentini, D. 2006, *Phys. Rev. Lett.*, 96, 061301

- Calibbi, L., Faccia, A., Masiero, A., & Vempati, S. K. 2006, *Phys. Rev. D*, 74, 116002
- Cooray, A. 1999, *A&A*, 348, 31
- Copeland, E. J., Sami, M., & Tsujikawa, S. 2006, *Int. J. Mod. Phys. D*, 15, 1753
- Cuoco, A., Iocco, F., Mangano, G., et al. 2004, *Int. J. Mod. Phys. A*, 19, 4431
- Crocce, M., & Scoccimarro, R. 2006, *Phys. Rev. D*, 73, 6
- De Bernardis, F., Serra, P., Cooray, A., & Melchiorri, A. 2008, *Phys. Rev. D*, 78, 083535
- Dunkley, J., Komatsu, E., Nolta, M. R., et al. 2009, *ApJS*, 180, 306
- Eisenstein, D. J., & Hu, W. 1998, *ApJ*, 496, 605
- Ellis, G. F. R. 1971, *Q. Jl. Astron. Soc.*, 16, 245
- Ellis, G. F. R., & Buchert, T. 2005, *Phys. Lett. A*, 347, 38
- Fardon, R., Nelson, A. E., & Weiner, N. 2004, *J. Cosmology Astropart. Phys.*, 10, 205
- Fogli, G. L., Lisi, E., Marrone, A., et al. 2008, *Phys. Rev. D*, 78, 033010
- Fu, L., Semboloni, E., Hoekstra, H., et al. 2008, *A&A*, 479, 9
- Gonzalez-Garcia, M. C., & Maltoni, M. 2008, *Phys. Rep.*, 460, 1
- Goobar, A., Hannestad, S., Moertsell, E., & Tu, H. 2006, *J. Cosmology Astropart. Phys.*, 06, 019
- Hannestad, S., Tu, H., & Wong, Y. 2006, *J. Cosmology Astropart. Phys.*, 06, 025
- Hastings, W. K. 1970, *Biometrika*, 57, 1
- Hirata, C., & Seljak, U. 2004, *Phys. Rev. D*, 70, 063526
- Hu, W., Eisenstein, D. J., & Tegmark, M. 1998, *Phys. Rev. Lett.*, 80, 5255
- Ichiki, K., Takada, M., & Takahashi, T. 2009, *Phys. Rev. D*, 79, 023520
- Ilbert, O., Arnouts, S., McCracken, H. J., et al. 2006, *A&A*, 457, 841
- Jing, Y. P., Zhang, P., Ling, W. P., Gao, L., & Springel, V. 2006, *ApJ*, 640, L119
- Kiakotou, A., Elgarøy, Ø., & Lahav, O. 2008, *Phys. Rev. D*, 77, 063005
- Kilbinger, M., Benabed, K., Guy, J., et al. 2009, *A&A*, 497, 677
- Kitching, T. D., Heavens, A. F., Verde, L., Serra, P., & Melchiorri, A. 2008, *Phys. Rev. D*, 77, 103008
- Kolb, E. W., Matarrese, S., & Riotto, A. 2006, *New J. Phys.*, 8, 322
- Komatsu, E., Dunkley, J., Nolta, M. R., et al. 2009, *ApJS*, 180, 330
- Kristiansen, J., Elgaroy, O., & Dahle, H. 2007, *Phys. Rev. D*, 75, 083510
- Lesgourgues, J., & Pastor, S. 2006, *Phys. Rep.*, 429, 307
- Lesgourgues, J., Pastor, S., & Perotto, L. 2004, *Phys. Rev. D*, 70, 045016
- Lewis, A., & Bridle, S. 2002, *Phys. Rev. D*, 66, 103511
- Mangano, G., Miele, G., Pastor, S., & Peloso, M. 2002, *Phys. Lett. B*, 534, 8
- Massey, R., Heymans, C., Berge, J., et al. 2007, *MNRAS*, 376, 13
- McTavish, C. J., Ade, P. A. R., Bode, J. J., et al. 2006, *ApJ*, 647, 799
- Munshi, D., Valageas, P., van Waerbeke, L., & Heavens, A. F. 2008, *Phys. Rep.*, 462, 67
- Peacock, J. A., & Dodds, S. J. 1996, *MNRAS*, 280, 19
- Peacock, J. A., Schneider, P., Efstathiou, G., et al. 2006, Report of the ESA-ESO Working Group on Fundamental Cosmology [arXiv:astro-ph/0610906]
- Percival, W. J., Cole, S., Eisenstein, D., et al. 2007, *MNRAS*, 381, 1053
- Pietroni, M. 2008, *JCAP*, 10, 036
- Riess, A. G., Strolger, L.-G., Tonry, J., et al. 2004, *ApJ*, 607, 665
- Ringwald, A., & Wong, Y. Y. 2004, *JCAP*, 0412, 005
- Saito, S., Takada, M., & Taruya, A. 2008, *Phys. Rev. Lett.*, 100, 191301
- Schneider, P., van Waerbeke, L., Jain, B., & Kruse, G. 1998, *MNRAS*, 296, 873
- Schneider, P., van Waerbeke, L., Kilbinger, M., & Mellier, Y. 2002, *A&A*, 396, 1
- Schimd, C., Uzan, J.-P., & Riazuelo, A. 2005, *Phys. Rev. D*, 71, 083512
- Schimd, C., Tereno, I., Uzan, J.-P., et al. 2007, *A&A*, 463, 405
- Seljak, U., Makarov, A., Mandelbaum, R., et al. 2005, *Phys. Rev. D*, 71, 043511
- Seljak, U., Slosar, A., McDonald, P., et al. 2006, *JCAP*, 10, 14
- Semboloni, E., van Waerbeke, L., Heymans, C., et al. 2007, *MNRAS*, 375, L6
- Semboloni, E., Tereno, I., van Waerbeke, L., & Heymans, C. 2008 [arXiv:0812.1881]
- Smith, R. E., Peacock, J. A., Jenkins, A., et al. 2003, *MNRAS*, 341, 1311
- Tegmark, M., Eisenstein, D. J., Strauss, M. A., et al. 2006, *Phys. Rev. D*, 74, 123507
- Tocchini-Valentini, D., & Amendola, L. 2002, *Phys. Rev. D*, 65, 063508
- Uzan, J.-P. 1999, *Phys. Rev. D*, 59, 123510
- Uzan, J.-P. 2006, *Gen. Rel. Grav.*, 39, 307
- Uzan, J.-P., Clarckson, C., & Ellis, G. F. R. 2008, *Phys. Rev. Lett.*, 100, 191303
- Wetterich, C. 1995, *A&A*, 301, 321
- White, M. 2005, *Astropart. Phys.*, 24, 334
- Wiltshire, D. 2007, *New J. Phys.*, 9, 377
- Wong, Y. Y. 2008, *JCAP*, 10, 035
- Zhan, H., & Knox, L. 2004, *ApJ*, 616, L75